

A Flexible Zero-Inflated Conway–Maxwell–Poisson Regression Model for Spatiotemporal Data of US Vaccine Refusal

Bokgyeong Kang¹, John Hughes², and Murali Haran¹

¹Department of Statistics, Pennsylvania State University

²College of Health, Lehigh University

Abstract

Vaccination is widely acknowledged as one of the most effective tools for preventing disease. However, there has been a rise in parental refusal and delay of childhood vaccination in recent years in the United States. This trend undermines the maintenance of herd immunity and elevates the likelihood of outbreaks of vaccine-preventable diseases. Our aim is to identify demographic or socioeconomic characteristics associated with vaccine refusal, which could help public health professionals and medical providers develop interventions targeted to concerned parents. We examine US county-level vaccine refusal data for patients under five years of age collected on a monthly basis during the period 2012–2015. These data exhibit challenging features: zero inflation, spatial dependence, seasonal variation, spatially-varying dispersion, and a large sample size (approximately 3,000 counties per month). We propose a flexible zero-inflated Conway–Maxwell–Poisson (ZICOMP) regression model that addresses these challenges. Because ZICOMP models have an intractable normalizing function, it is challenging to do Bayesian inference for these models. We propose a new hybrid Monte Carlo algorithm that permits efficient sampling and provides asymptotically exact estimates of model parameters.

Keywords: High-dimensional spatial model; Spatially-varying dispersion; Vaccine refusal; Zero inflation; Bayesian spatial filtering; Exchange algorithm.

1 Introduction

Childhood vaccination coverage has remained high in the United States. However, due to recent outbreaks of childhood vaccine-preventable diseases in the United States, there is still increased public health concern regarding the upward trend of vaccine refusal and hesitancy. The Centers for Disease Control and Prevention (CDC) reported that 1,274 individual cases of measles were confirmed across 31 states in 2019. This is the greatest number of cases reported in a single year since 1992. And the incidence of pertussis has been steadily increasing since it reached its lowest point in 1976. A significant proportion of the cases were found to be among unvaccinated or undervaccinated individuals. Communities with higher vaccine exemption rates have higher incidence rates of the diseases (Phadke et al., 2016; Patel et al., 2019). It is important to identify communities' demographic or socioeconomic characteristics associated with vaccine refusal. This could help public health professionals and medical providers develop interventions targeted to concerned communities.

There is a large literature on vaccine uptake for childhood infections in the United States. Most studies have relied on the CDC's National Immunization Survey (NIS) data or school vaccination exemption records. These studies have been limited in spatial resolution or scale. The NIS data are representative and comparable across states but have low spatial resolution (state-level) and low response rates (Smith et al., 2004; Salmon et al., 2006; Frieden et al., 2014; Hill et al., 2015). School vaccination exemption records have finer spatial resolution and high response rates but are available for only a small number of states (Zipfel et al., 2020). A limited number of studies have used claims data where vaccination status were assessed using ICD-9 codes (McCarthy et al., 2013; Glanz et al., 2013; Lieu et al., 2015). However, these studies have been small in scale.

In this manuscript we examine large-scale high-resolution childhood vaccine refusal data (Kang et al., 2022). These data represent county-level monthly incidence of childhood vaccine refusal across the United States from 2012 to 2015 obtained from data managed by IMS Health. The dataset includes county-level demographic and socioeconomic characteristics that are hypothesized determinants of vaccine refusal. Kang et al. (2022) aggregated the data by year to remove seasonality. To avoid information loss due to aggregation, we

use the original data. These data exhibit challenging features. First, there is an excess of zeros. Over 79% of the counties recorded no refusals in any given month. Second, vaccine refusal has been shown to exhibit seasonal variation since high incidences of vaccine refusal are observed during the first few months of school. Third, vaccine refusal behavior has been found to be spatially clustered. We observe that the high incidences of vaccine refusal are clustered. Fourth, the dispersion of the refusal counts may vary over space. Our exploratory analysis suggests that some counties may be under-dispersed and some may be over-dispersed. Finally, the sample size is large. There are approximately 3,000 observations in any given month. This makes Markov chain Monte Carlo (MCMC) algorithms for these data computationally demanding due to large-matrix operations and slow mixing of spatial random effects. These challenges motivate the development of a new, flexible model and an efficient computational method.

In this article we propose a new zero-inflated Conway–Maxwell–Poisson (ZICOMP) regression model and several computational methods that address the above mentioned challenges. We include spatially dependent random effects that account for the spatial clustering of refusal and for spatially-varying dispersion. The spatial effects are modeled via a Bayesian spatial filtering (BSF) approach (Hughes, 2017), which represents the random effects with linear combinations of spatially patterned basis functions. This BSF method addresses key computational challenges by reducing the dimension of and correlation among the spatial random effects. Previous studies have used information criteria or cross-validation for choosing the best basis vectors. However, these approaches require fitting a model multiple times for various subsets of the basis vectors, which can be computationally expensive. We propose to choose suitable basis vectors using a reversible jump MCMC (Green, 1995; Godsill, 2012) algorithm. Bayesian inference for the class of ZICOMP models is challenging due to an intractable normalizing function. We propose an efficient new hybrid Monte Carlo algorithm that also yields asymptotically exact inference, i.e., we sample from a Markov chain whose stationary distribution is exactly equal to the target distribution.

The remainder of this article is organized as follows. In Section 2 we describe the

vaccine refusal data. In Section 3 we specify our ZICOMP model. In Section 4 we present our hybrid Monte Carlo algorithm. In Section 5 we discuss simulation experiments for our proposed model and computational approach. In Section 6 we analyze the vaccine refusal data. We conclude in Section 7.

2 Vaccine refusal data

Reports for vaccine refusal among patients under five years of age were obtained from a database of U.S. medical claims managed by IMS Health on a monthly basis from 2012 to 2015. Claims were submitted from both private and government insurance providers, and data were aggregated according to U.S. five-digit ZIP codes. The reported data cover

Table 1: Description of the covariate variables.

Variable	Description
<i>Measurement variables</i>	
Physician-patient interactions	Number of physician-patient interactions
Health insurance	Proportion of people with health insurance
Pediatrician reporting	Rate at which a pediatrician voluntarily reports non-billable diagnoses
<i>Demographic or socioeconomic variables</i>	
Household size	Average number of individuals living in a single household
Religious congregations	Per capita number of congregations of religions historically opposed to vaccination
Limited English proficiency	Proportion of people who are not proficient in English
Private school	Proportion of children who attend private school
High income	Proportion of people in the upper 20% quantile of income in the US
Same area	Proportion of people living in the same county one year prior
State law leniency	Exemption law effectiveness index
State autism	Among families with more than 1 child, the proportion with a current or past diagnosis of autism

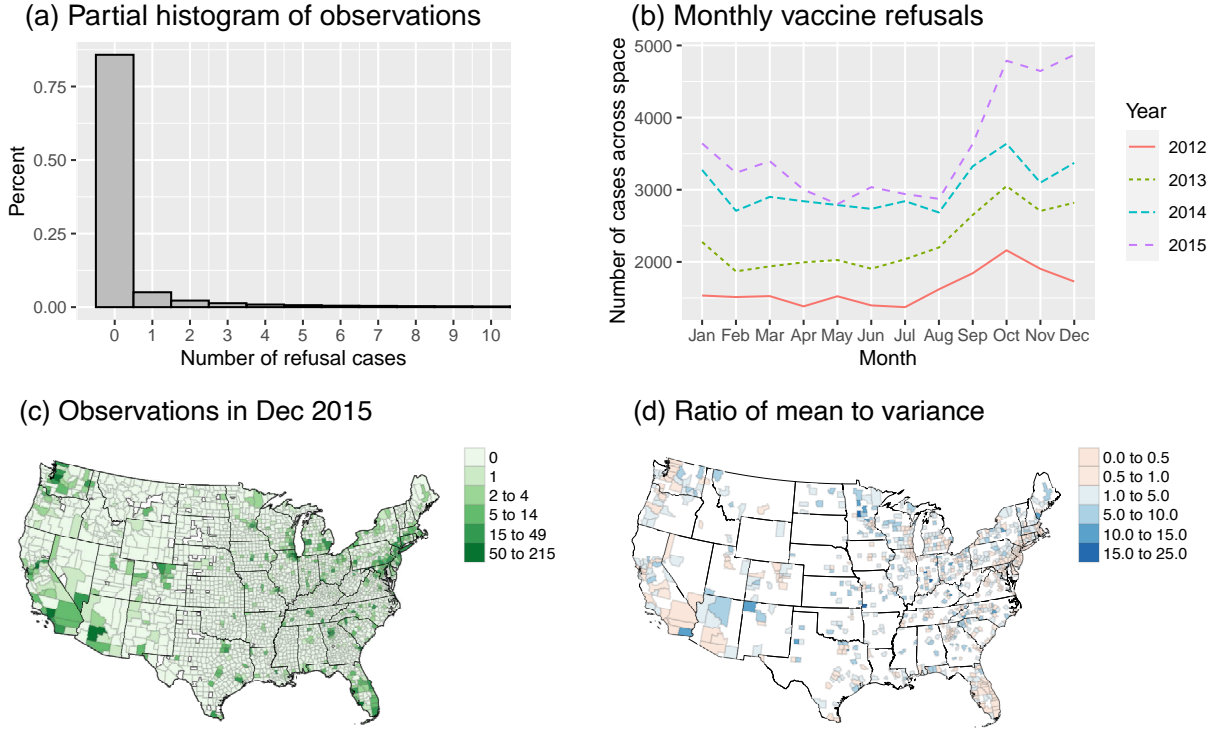


Figure 1: (a) Partial histogram of refusal incidence (up to 10 cases). (b) Monthly incidence of refusal aggregated across space. (c) Refusal incidence observed in December 2015. (d) Ratio of sample mean to variance of positive counts across time for each county.

126,049 cases of vaccine refusal for children under the age of five across 2,470,596,759 physician-patient interactions. Vaccine refusal was identified with the International Classification of Disease, Ninth Revision (ICD-9) code and sub-codes for “vaccination not carried out” (V64.0). Thus a vaccine refusal represents a case when a patient was not immunized due to philosophical or religious reasons.

There are four conditions, all of which would have to be met for a vaccine refusal to be captured in the database: (1) an individual seeks pediatric health care from a provider, (2) the individual is insured, (3) the provider uses the claims database, and (4) the provider reports the vaccine refusal. The set of covariate variables includes factors representing these measurement mechanisms (top of Table 1) and county-level demographic or socioeconomic factors that are hypothesized determinants of vaccine refusal (bottom of Table 1). The

data set contains records for approximately 3,000 counties for each month. All explanatory variables were centered and standardized for use in the model.

Several salient features of the data must be considered when formulating a statistical model. First, the observations are potentially zero-inflated. Figure 1 (a) shows the partial histogram of observed outcomes. Approximately 86% of outcomes are zeros, and over 79% of the counties reported no refusals in a given month. Some of the zeros may have been produced by imperfect detection of refusal due to spatial variation in healthcare access and insurance rates. An appropriate model should account for imperfect detection. Second, childhood vaccine refusal has been shown to exhibit seasonal variation. This is mainly caused by state-mandated school entry immunization requirements in the United States. Figure 1 (b) displays the monthly incidence of refusal aggregated across space. It is observed that the incidence tends to rise during the first few months of the school year. An appropriate model should accommodate this seasonal pattern. Third, vaccine refusal behavior has been shown to exhibit spatial clustering. Figure 1 (c) shows the outcomes observed in December 2015. It is observed that counties with high incidence are clustered. Similar results are observed for the other months. This indicates that our model should provide spatial smoothing and borrowing of information among adjacent regions. Fourth, the data are potentially over- and under-dispersed. Figure 1 (d) shows the ratio of sample mean to variance of positive counts across time for each county. Some counties have ratio values less than 1, which implies potential over-dispersion. Some have ratio values greater than 1, indicating possible under-dispersion. Thus a suitable model should accommodate both over- and under-dispersed, and should permit the dispersion to vary over space. Finally, the data size is large—approximately 3,000 observations in any given month. Our model and inferential approach should handle this large data set efficiently.

3 Zero-inflated Conway–Maxwell–Poisson regression model

In this section we introduce a new model and several computational innovations that together address the challenging features of the data described in Section 2. We begin with a description of the well known Conway–Maxwell–Poisson (COMP) distribution and build upon it to first handle zero-inflated spatial regression and spatially varying dispersion. Then we incorporate spatial filtering to greatly reduce the computational burden. Finally, we complete our model specification by introducing indicator variables that facilitate basis-vector selection via reversible jump MCMC.

3.1 Conway–Maxwell–Poisson distribution

The Conway–Maxwell–Poisson (COMP) distribution (Conway and Maxwell, 1962) is a two-parameter generalization of the Poisson distribution that allows for under-dispersion (variance less than the mean), equi-dispersion (variance equals the mean), and over-dispersion (variance greater than the mean). A count variable Y is said to follow the $\text{COMP}(\lambda, \nu)$ distribution if Y 's probability mass function (pmf) is

$$P(Y = y) = \frac{1}{c(\lambda, \nu)} \frac{\lambda^y}{(y!)^\nu},$$

where $\lambda > 0$ is a generalization of the Poisson rate parameter, $\nu \geq 0$ is the dispersion parameter, and $c(\lambda, \nu) = \sum_{z=0}^{\infty} \lambda^z / (z!)^\nu$ is a normalizing function. There is under-dispersion when $\nu > 1$; there is equi-dispersion when $\nu = 1$; and there is over-dispersion when $0 \leq \nu < 1$. The COMP distribution contains three classical count distributions as special cases: Poisson ($\nu = 1$), geometric ($\nu = 0$, $\lambda < 1$, and success probability $1 - \lambda$), and Bernoulli ($\nu = \infty$ and success probability $\lambda / (1 + \lambda)$). We use a reparameterization introduced by Guikema and Goffelt (2008) that substitutes $\eta = \lambda^{1/\nu}$ to approximate the center of the COMP distribution. A variable Y is said to follow the $\text{COMP}_\eta(\eta, \nu)$ distribution if Y 's

pmf is

$$P(Y = y) = \frac{1}{c_\eta(\eta, \nu)} \left(\frac{\eta^y}{y!} \right)^\nu,$$

with $c_\eta(\eta, \nu) = \sum_{z=0}^{\infty} (\eta^z/z!)^\nu$. The mode of this distribution is $\lfloor \eta \rfloor$. Shmueli et al. (2005) approximated the mean and variance by

$$\mathbb{E}(Y) \approx \eta + \frac{1}{2\nu} - \frac{1}{2}, \quad \mathbb{V}(Y) \approx \frac{\eta}{\nu}. \quad (1)$$

These approximations are close for a wide range of η and ν .

3.2 ZICOMP regression model

A zero-inflated model (Lambert, 1992) comprises two processes: a binary process and a count process. The binary process is a point mass at zero and accounts for excess zeros. The count process follows a distribution that can explain the remaining zeros and positive observations. In the context of our application, examining vaccine refusal incidence, the binary process classifies the entire data set into two groups: a missing data group and a detected refusal group. The missing data group contains zeros, and those zeros represent the fact that some people refused vaccination but those refusals were not captured in the database. The detected refusal group consists of positive observations and the remaining zeros, and those zeros mean there were no refusals. The observations in the detected refusal group are described by the count process. For the count process we use the COMP distribution so we can account for under- and over-dispersion in the data.

Modeling these two processes together leads to the zero-inflated Conway–Maxwell–Poisson (ZICOMP) distribution, which has pmf

$$P(Y_{st} = y_{st}) = (1 - \pi_{st}) \mathbb{1}_{\{w_{st}=0, y_{st}=0\}} + \pi_{st} p(y_{st}; \eta_{st}, \nu_s) \mathbb{1}_{\{w_{st}=1\}}$$

$$s = 1, \dots, n; \quad t = 1, \dots, T,$$

where y_{st} denotes the observed response at spatial location s and time t , $p(\cdot; \eta_{st}, \nu_s)$ is the

pmf of the $\text{COMP}_\eta(\eta_{st}, \nu_s)$ distribution, π_{st} is the probability of y_{st} being in the detected refusal group, and $w_{st} \sim \text{Bernoulli}(\pi_{st})$ indicates whether y_{st} is in the detected group. We model the parameters as follows:

$$\begin{aligned}\text{logit}(\pi_{st}) &= \mathbf{X}_{st}^\top \boldsymbol{\beta}_1 \\ \log(\eta_{st}) &= \mathbf{X}_{st}^\top \boldsymbol{\beta}_2 + V_s + \mathbf{M}_t^\top \boldsymbol{\zeta} \\ \log(\nu_s) &= \alpha + W_s,\end{aligned}$$

where \mathbf{X}_{st} is a vector consisting of an intercept and covariate values for location s and time t , $\boldsymbol{\beta}_1$ and $\boldsymbol{\beta}_2$ are regression coefficients, V_s and W_s are spatial random effects for location s , \mathbf{M}_t is a vector of 11 dummy variables for month fixed effects, $\boldsymbol{\zeta}$ are their coefficients, and α is an intercept for dispersion. The dispersion is constant across space if $W_s = 0$ for $s = 1, \dots, n$. We assume that the fields of spatial random effects are independent between the approximate modes $\boldsymbol{\eta}$ and dispersions $\boldsymbol{\nu}$, i.e., $\mathbf{V} = (V_1, \dots, V_n)^\top$ is independent of $\mathbf{W} = (W_1, \dots, W_n)^\top$.

The conditional autoregressive (CAR) model is a traditional choice of prior distribution for spatial random effects (Besag, 1974). The CAR priors for the spatial random fields \mathbf{V} and \mathbf{W} are given by

$$\mathbf{V} \mid \kappa \sim \text{Normal}_n(\mathbf{0}, \mathbf{Q}^{-1}/\kappa) \quad (2)$$

$$\mathbf{W} \mid \tau \sim \text{Normal}_n(\mathbf{0}, \mathbf{Q}^{-1}/\tau), \quad (3)$$

where κ and τ are smoothing parameters and $\mathbf{Q} = \text{diag}(\mathbf{A}\mathbf{1}) - \rho\mathbf{A}$ is a precision matrix where \mathbf{A} is the adjacency matrix of the underlying graph, $\mathbf{1}$ is the conformable vector of 1s, and $\rho \in [0, 1)$ indicates the strength of spatial correlation ($\rho = 0$ implies spatial independence while ρ near 1 implies strong spatial correlation). Note that \mathbf{Q} intuitively accounts for both dependences (V_i and V_j , $i \neq j$, are independent given their neighbors if and only if $(\mathbf{Q})_{ij} = (\mathbf{Q})_{ji} = 0$ if and only if locations i and j are not adjacent) and prior uncertainty (uncertainty about V_i is inversely proportional to the number of neighbors of location i : $(\mathbf{Q})_{ii} = (\mathbf{A})_i\mathbf{1}$ where $(\mathbf{A})_i$ denotes the i th row of \mathbf{A}). Markov chain Monte Carlo

(MCMC) is a standard approach for estimating the random effects. However, in this setting MCMC is computationally burdensome for a large sample size n , owing to costly ($\mathcal{O}(n^3)$) evaluations of n -dimensional multivariate normal likelihood functions at each iteration. Additionally, strong correlations among the spatial random effects can lead to slow mixing chains (Haran, 2011). Using the CAR model for our data is impractical since there are $n \approx 3,000$ counties in a given month.

3.3 ZICOMP with spatial filtering

To reduce the dimensions of and the correlations among the spatial random effects, we reparameterize the spatial random effects as linear combinations of basis vectors:

$$\begin{aligned} \mathbf{V} &= \mathbf{B}\boldsymbol{\gamma}^* \\ \mathbf{W} &= \mathbf{B}\boldsymbol{\delta}^*, \end{aligned}$$

where \mathbf{B} is a basis matrix the columns of which are $q \ll n$ basis vectors, and $\boldsymbol{\gamma}^*$ and $\boldsymbol{\delta}^*$ are basis coefficients. There are two common choices of \mathbf{B} : (1) in restricted spatial regression (RSR), the spatial basis vectors are constrained to be orthogonal to the fixed-effects predictors (cf. Reich et al., 2006; Hughes and Haran, 2013); and (2) in Bayesian spatial filtering (BSF), the spatial basis vectors are constrained to be orthogonal to the intercept (Hughes, 2017). The RSR models have been found to yield low coverage rates for the regression coefficients (Hanks et al., 2015; Khan and Calder, 2020; Zimmerman and Hoef, 2021). Our simulation experiments showed that the BSF parameterization does not adversely impact inference for the regression coefficients, and so we employ the BSF approach.

Specifically, the BSF basis matrix \mathbf{B} comprises selected eigenvectors of $\mathbf{F} = (\mathbf{I} - \mathbf{1}\mathbf{1}^\top/n)\mathbf{A}(\mathbf{I} - \mathbf{1}\mathbf{1}^\top/n)$, where \mathbf{I} is the $n \times n$ identity matrix and $\mathbf{1}$ is the n -dimensional vector of 1s. The eigenvectors of \mathbf{F} comprise all possible mutually distinct patterns that can arise on the graph and hence can be used to model a spatial random field. The positive (negative) eigenvalues of \mathbf{F} correspond to varying degrees of attractive (repulsive) spatial dependence. An eigenvector's pattern has finer scale with decreasing magnitude of the

corresponding eigenvalue. In other words, \mathbf{B} can accommodate spatial structure at multiple scales. We henceforth assume that \mathbf{B} comprises the first $q \ll n$ basis vectors since we expect neighboring observations to be similar (i.e., we discard all of the repulsive patterns). The priors for the basis coefficients are given by

$$\begin{aligned}\boldsymbol{\gamma}^* \mid \kappa &\sim \text{Normal}_q(\mathbf{0}, \mathbf{Q}_B^{-1}/\kappa) \\ \boldsymbol{\delta}^* \mid \tau &\sim \text{Normal}_q(\mathbf{0}, \mathbf{Q}_B^{-1}/\tau),\end{aligned}$$

where $\mathbf{Q}_B = \mathbf{B}^\top \mathbf{Q} \mathbf{B}$. This allows for $\mathbf{B}\boldsymbol{\gamma}^*$ and $\mathbf{B}\boldsymbol{\delta}^*$ to stand in for the CAR effects in (2) and (3), respectively. The number q of basis vectors has been decided via information criteria or cross-validation. However, these approaches require fitting the model multiple times for various choices of q . This can be too computationally demanding for big data.

We use a reversible jump MCMC approach to allow for automatic selection of suitable basis vectors. We introduce latent variables indicating whether basis vectors are included in the model. Let $\boldsymbol{\gamma}^* = (\gamma_1^*, \dots, \gamma_q^*)^\top$ and $\boldsymbol{\delta}^* = (\delta_1^*, \dots, \delta_q^*)^\top$. For $j = 1, \dots, q$, we reparameterize the basis coefficients γ_j^* and δ_j^* as

$$\begin{aligned}\gamma_j^* &= \gamma_j I_{\gamma_j} \\ \delta_j^* &= \delta_j I_{\delta_j},\end{aligned}$$

where I_{γ_j} and I_{δ_j} are 1 if the j th basis vector is suitable, and they are 0 otherwise. Let $\boldsymbol{\gamma} = (\gamma_1, \dots, \gamma_q)^\top$, $\boldsymbol{\delta} = (\delta_1, \dots, \delta_q)^\top$, $\mathbf{I}_\gamma = \text{diag}[(I_{\gamma_1}, \dots, I_{\gamma_q})^\top]$, and $\mathbf{I}_\delta = \text{diag}[(I_{\delta_1}, \dots, I_{\delta_q})^\top]$.

Then our proposed model is given by

$$\begin{aligned}
y_{st} & \begin{cases} = 0 & \text{w.p. } 1 - \pi_{st} \\ \sim \text{COMP}_{\eta}(\eta_{st}, \nu_s) & \text{w.p. } \pi_{st}, \end{cases} \\
\text{logit}(\pi_{st}) &= \mathbf{X}_{st}^{\top} \boldsymbol{\beta}_1 \\
\log(\eta_{st}) &= \mathbf{X}_{st}^{\top} \boldsymbol{\beta}_2 + \mathbf{B}_s^{\top} \boldsymbol{\gamma} \mathbf{I}_{\gamma} + \mathbf{M}_t^{\top} \boldsymbol{\zeta} \\
\log(\nu_s) &= \alpha + \mathbf{B}_s^{\top} \boldsymbol{\delta} \mathbf{I}_{\delta}, \\
s &= 1, \dots, n; \quad t = 1, \dots, T,
\end{aligned}$$

where \mathbf{B}_s is the q -dimensional vector of basis function values corresponding to location s .

4 A hybrid Monte Carlo algorithm for our ZICOMP model

In this section we propose a hybrid Monte Carlo algorithm that combines several Monte Carlo algorithms to provide asymptotically exact estimates of our model parameters. Standard MCMC cannot be used for our model due to the intractable normalizing function of the COMP distribution. We employ an exchange algorithm (Murray et al., 2006) that was developed for carrying out inference in the presence of intractable normalizing functions. We introduce a proposal distribution that allows for the algorithm to perform better for zero-inflated models.

4.1 Computational challenge

Let $\boldsymbol{\theta} = (\mathbf{w}, \boldsymbol{\beta}_1, \boldsymbol{\beta}_2, \boldsymbol{\zeta}, \alpha, \boldsymbol{\gamma}, \boldsymbol{\delta}, \mathbf{I}_{\gamma}, \mathbf{I}_{\delta}, \kappa, \tau)$ be the collection of model parameters. The joint posterior distribution of $\boldsymbol{\theta}$ is given by

$$\begin{aligned}
\pi(\boldsymbol{\theta} \mid \mathbf{y}) &\propto p(\boldsymbol{\theta}) L(\boldsymbol{\theta} \mid \mathbf{y}) \\
&= p(\boldsymbol{\theta}) \prod_{s=1}^n \prod_{t=1}^T (1 - \pi_{st})^{1-w_{st}} \left\{ \frac{\pi_{st}}{c_{\eta}(\eta_{st}, \nu_s)} \left(\frac{\eta_{st}^{y_{st}}}{y_{st}!} \right)^{\nu_s} \right\}^{w_{st}},
\end{aligned}$$

where $p(\boldsymbol{\theta})$ denotes a prior density and $L(\boldsymbol{\theta} \mid \mathbf{y})$ represents the likelihood function for our model. Let $\boldsymbol{\theta}_i$ be a subset of the parameters and $\boldsymbol{\theta}_{-i}$ denote the rest of the parameters. The full conditional posterior distribution of $\boldsymbol{\theta}_i$ is given by

$$\pi(\boldsymbol{\theta}_i \mid \boldsymbol{\theta}_{-i}, \mathbf{y}) \propto p(\boldsymbol{\theta}_i) L(\boldsymbol{\theta}_i \mid \boldsymbol{\theta}_{-i}, \mathbf{y}),$$

where $p(\boldsymbol{\theta}_i)$ is a prior density and $L(\boldsymbol{\theta}_i \mid \boldsymbol{\theta}_{-i}, \mathbf{y})$ is obtained by removing all terms not involving $\boldsymbol{\theta}_i$ from $L(\boldsymbol{\theta} \mid \mathbf{y})$. Consider the full conditional $\pi(\boldsymbol{\theta}_i \mid \boldsymbol{\theta}_{-i}, \mathbf{y})$. The Metropolis-Hastings (MH) algorithm proposes $\boldsymbol{\theta}'_i$ from $q(\cdot \mid \boldsymbol{\theta}_i)$ and accepts $\boldsymbol{\theta}'_i$ with probability

$$\alpha(\boldsymbol{\theta}'_i \mid \boldsymbol{\theta}_i) = \min \left\{ 1, \frac{p(\boldsymbol{\theta}'_i) L(\boldsymbol{\theta}'_i \mid \boldsymbol{\theta}_{-i}, \mathbf{y}) q(\boldsymbol{\theta}_i \mid \boldsymbol{\theta}'_i)}{p(\boldsymbol{\theta}_i) L(\boldsymbol{\theta}_i \mid \boldsymbol{\theta}_{-i}, \mathbf{y}) q(\boldsymbol{\theta}'_i \mid \boldsymbol{\theta}_i)} \right\},$$

at each step of the algorithm. Gibbs sampling is a special case of the MH algorithm where we can generate samples exactly from $\pi(\boldsymbol{\theta}_i \mid \boldsymbol{\theta}_{-i}, \mathbf{y})$. We use an MH update for $\boldsymbol{\beta}_1$ and Gibbs updates for smoothing parameters κ and τ .

Standard MCMC cannot be used for the other parameters, however. Consider parameters besides $\boldsymbol{\beta}_1$, κ , and τ . Then the full conditional of $\boldsymbol{\theta}_i$ is given by

$$\pi(\boldsymbol{\theta}_i \mid \boldsymbol{\theta}_{-i}, \mathbf{y}) \propto p(\boldsymbol{\theta}_i) \prod_{s=1}^n \prod_{t=1}^T (1 - \pi_{st})^{1-w_{st}} \left\{ \frac{\pi_{st}}{c_\eta(\eta_{st}, \nu_s)} \left(\frac{\eta_{st}^{y_{st}}}{y_{st}!} \right)^{\nu_s} \right\}^{w_{st}}.$$

Let $h(\mathbf{y} \mid \boldsymbol{\theta}) = \prod_{s=1}^n \prod_{t=1}^T (\eta_{st}^{y_{st}} / y_{st}!)^{\nu_s w_{st}}$ be an unnormalized likelihood and $r(\boldsymbol{\theta}) = \prod_{s=1}^n \prod_{t=1}^T (1 - \pi_{st})^{1-w_{st}} \{ \pi_{st} / c_\eta(\eta_{st}, \nu_s) \}^{w_{st}}$ be its normalizing constant. The normalizing constant $r(\boldsymbol{\theta})$ is intractable since $c_\eta(\eta_{st}, \nu_s)$ is an infinite sum. The MH acceptance probability becomes

$$\alpha(\boldsymbol{\theta}'_i \mid \boldsymbol{\theta}_i) = \min \left\{ 1, \frac{p(\boldsymbol{\theta}'_i) h(\mathbf{y} \mid \boldsymbol{\theta}') r(\boldsymbol{\theta}) q(\boldsymbol{\theta}_i \mid \boldsymbol{\theta}'_i)}{p(\boldsymbol{\theta}_i) h(\mathbf{y} \mid \boldsymbol{\theta}) r(\boldsymbol{\theta}') q(\boldsymbol{\theta}'_i \mid \boldsymbol{\theta}_i)} \right\},$$

where $\boldsymbol{\theta}' = (\boldsymbol{\theta}'_i, \boldsymbol{\theta}_{-i})$. The intractable normalizing constant $r(\boldsymbol{\theta})$ does not cancel out in the acceptance probability. Thus standard MCMC techniques cannot be applied. We sidestep this problem by introducing an auxiliary variable as described in the following section.

4.2 An exchange algorithm for our ZICOMP model

Murray et al. (2006) introduced an auxiliary variable \mathbf{z} that follows $h(\mathbf{z} \mid \boldsymbol{\theta}')/r(\boldsymbol{\theta}')$ so that the intractable terms cancel out in the MH acceptance probability. Consider the full conditional $\pi(\boldsymbol{\theta}_i \mid \boldsymbol{\theta}_{-i}, \mathbf{y})$. The exchange algorithm proceeds as follows: given $\boldsymbol{\theta}_i$,

1. propose $\boldsymbol{\theta}'_i \sim q(\cdot \mid \boldsymbol{\theta}_i)$,
2. generate an auxiliary variable exactly from the probability model at $\boldsymbol{\theta}'$: $\mathbf{z} \sim \frac{h(\cdot \mid \boldsymbol{\theta}')}{r(\boldsymbol{\theta}')}$, and
3. accept $\boldsymbol{\theta}'_i$ with probability

$$\alpha = \min \left\{ 1, \frac{p(\boldsymbol{\theta}'_i)h(\mathbf{y} \mid \boldsymbol{\theta}')\cancel{r(\boldsymbol{\theta})}h(\mathbf{z} \mid \boldsymbol{\theta})\cancel{r(\boldsymbol{\theta}')}q(\boldsymbol{\theta}_i \mid \boldsymbol{\theta}'_i)}{p(\boldsymbol{\theta}_i)h(\mathbf{y} \mid \boldsymbol{\theta})\cancel{r(\boldsymbol{\theta}')}h(\mathbf{z} \mid \boldsymbol{\theta}')\cancel{r(\boldsymbol{\theta})}q(\boldsymbol{\theta}'_i \mid \boldsymbol{\theta}_i)} \right\}.$$

We see that the normalizing constants cancel in the acceptance probability. We note that the exchange algorithm provides asymptotically exact estimates of model parameters. We use the exchange algorithm for $\boldsymbol{\beta}_2$, $\boldsymbol{\zeta}$, α , $\boldsymbol{\gamma}$, $\boldsymbol{\delta}$, \mathbf{I}_γ , and \mathbf{I}_δ . A fast rejection sampling scheme for COMP distributions (Chanialidis et al., 2018; Benson and Friel, 2021) can be used for generating an auxiliary variable in Step 2.

However, we cannot use this method for the detection indicator variables \mathbf{w} . If $y_{st} > 0$, then $w_{st} = 1$ with probability 1, by definition. If $y_{st} = 0$, then we observe either missing data (implying $w_{st} = 0$) or a detected zero (implying $w_{st} = 1$). Conditional on $y_{st} = 0$, the full conditional of $\boldsymbol{\theta}_i = w_{st}$ is given by

$$\pi(w_{st} \mid \boldsymbol{\theta}_{-i}, y_{st} = 0) \propto p(w_{st})(1 - \pi_{st})^{1-w_{st}} \left\{ \frac{\pi_{st}}{c_\eta(\eta_{st}, \nu_s)} \right\}^{w_{st}},$$

where $p(w_{st})$ is a prior density. Given $w_{st} = 1$, the full conditional is proportional to the intractable COMP normalizing function $c_\eta(\eta_{st}, \nu_s)$. We propose w'_{st} from the swapping distribution $q(\cdot \mid w_{st}) = \delta(1 - w_{st} - \cdot)$, where δ denotes the Dirac delta function. Suppose we generate an auxiliary variable according to

$$z_{st} \begin{cases} = 0 & \text{if } w'_{st} = 0 \\ \sim \text{COMP}_\eta(\eta_{st}, \nu_s) & \text{if } w'_{st} = 1. \end{cases}$$

Suppose $w_{st} = 0$. Then the algorithm proposes $w'_{st} = 1$, generates an auxiliary variable $z_{st} \sim \text{COMP}_\eta(\eta_{st}, \nu_s)$, and accepts $w'_{st} = 1$ with probability

$$\begin{aligned} \alpha(w'_{st} = 1 \mid w_{st} = 0) &= \min \left\{ 1, \frac{p(w'_{st}) \frac{\pi_{st}}{c_\eta(\eta_{st}, \nu_s)} \delta(z_{st})}{p(w_{st})(1 - \pi_{st}) \frac{1}{c_\eta(\eta_{st}, \nu_s)} \left(\frac{\eta_{st}^{z_{st}}}{z_{st}!} \right)^{\nu_s}} \right\}, \\ &= \min \left\{ 1, \frac{p(w'_{st}) \pi_{st} \delta(z_{st})}{p(w_{st})(1 - \pi_{st}) \left(\frac{\eta_{st}^{z_{st}}}{z_{st}!} \right)^{\nu_s}} \right\}. \end{aligned}$$

The acceptance probability $\alpha(w'_{st} = 1 \mid w_{st} = 0) = 0$ whenever $z_{st} > 0$. In practice, when there is severe over-dispersion, the probability of accepting $w'_{st} = 1$ becomes very small, leading to an impractical algorithm. We can address this problem by introducing the following mixture distribution for the auxiliary variable:

$$z_{st} \sim \begin{cases} \text{NB}(\eta_{st}, \nu_s) & \text{if } w'_{st} = 0 \\ \text{COMP}_\eta(\eta_{st}, \nu_s) & \text{if } w'_{st} = 1, \end{cases} \quad (4)$$

where $\text{NB}(a, b)$ denotes the negative binomial distribution with mean a and dispersion b . To simplify the description of our acceptance ratio, let

$$g(z_{st} \mid \boldsymbol{\theta}') = \left\{ \frac{\Gamma(z_{st} + \nu_s)}{\Gamma(z_{st} + 1)\Gamma(\nu_s)} \left(\frac{\nu_s}{\eta_{st} + \nu_s} \right)^{\nu_s} \left(\frac{\eta_{st}}{\eta_{st} + \nu_s} \right)^{z_{st}} \right\}^{1-w'_{st}} \left\{ \frac{\eta_{st}^{z_{st}}}{z_{st}!} \right\}^{\nu_s w'_{st}},$$

where $\boldsymbol{\theta}' = (w'_{st}, \boldsymbol{\theta}_{-i})$. An exchange algorithm with the proposal distribution (4) for the auxiliary variable accepts w'_{st} with probability

$$\alpha(w'_{st} \mid w_{st}) = \min \left\{ 1, \frac{p(w'_{st})(1 - \pi_{st})^{1-w'_{st}} \pi_{st}^{w'_{st}} g(z_{st} \mid \boldsymbol{\theta}')}{p(w_{st})(1 - \pi_{st})^{1-w_{st}} \pi_{st}^{w_{st}} g(z_{st} \mid \boldsymbol{\theta}')} \right\}.$$

We found that this algorithm performed well in our simulation experiments.

4.3 A hybrid Monte Carlo algorithm

Here we summarize our hybrid Monte Carlo algorithm. The algorithm proceeds as follows.

1. Use an exchange algorithm for w_{st} for $s = 1, \dots, n$ and $t = 1, \dots, T$. The proposal for the auxiliary variable is given in (4).
2. Use a MH update for β_1 .
3. Use an exchange algorithm for $\beta_2, \zeta, \alpha, \gamma$, and δ . The proposal for the auxiliary variable is our ZICOMP model.
4. Use an exchange algorithm for I_{γ_j} and I_{δ_j} for $j = 1, \dots, q$. The proposal for the auxiliary variable is our ZICOMP model.
5. Do Gibbs updates for κ and τ .

The proposed algorithm generates a Markov chain whose stationary distribution is exactly equal to the posterior distribution of interest. We generate the auxiliary variable in parallel in Steps 1, 3, and 4. It can be computationally demanding to update I_{γ_j} and I_{δ_j} for $j = 1, \dots, q$ at every iteration for big data. To speed up computation, we randomly select m basis vectors and update only those indicator variables for a given iteration. Alternatively, we could update all variables at every k th iteration. To our knowledge, no existing theory suggests that the latter approach is asymptotically exact. But we found that this method produces faster convergence than the former method and correctly chooses the true basis vectors. And so we use the latter method in the sequel.

5 Applications to simulated data

Here we apply our ZICOMP model to data simulated from (i) a full model with spatial and temporal effects and spatially-varying dispersion, (ii) a model with constant dispersion, i.e., $\delta = \mathbf{0}$, (iii) a model with fixed effects only, i.e., $\gamma = \delta = \mathbf{0}$, and (iv) a model with covariate effects only, i.e., $\gamma = \delta = \zeta = \mathbf{0}$. An aim of the simulation experiments is to assess how our model and computational approach perform in the context of data generated from models with varying degrees of spatial and temporal dependence. The underlying graph for the data is the 30×30 lattice. Our design matrix is $\mathbf{X}_t = [\mathbf{1} \ \mathbf{x}_1 \ \mathbf{x}_2]$ for $t = 1, \dots, T$, where $\mathbf{x}_1 = (x_{1,1}, \dots, x_{1,900})^\top$ and $\mathbf{x}_2 = (x_{2,1}, \dots, x_{2,900})^\top$ are the x- and y-coordinates of

the vertices. We restrict the coordinates of the vertices to the unit square. We use the first 25 eigenvectors of \mathbf{F} to simulate data for our study, i.e., $\dim(\boldsymbol{\gamma}) = \dim(\boldsymbol{\delta}) = 25$ and \mathbf{B} is 900×25 . We simulate $T = 24$ observations per vertex for a total of $N = 900 \times 24 = 21,600$ observations.

We assume independent $N(\mathbf{0}, 100\mathbf{I})$ priors for the fixed effects $\boldsymbol{\beta}_1$, $\boldsymbol{\beta}_2$, $\boldsymbol{\zeta}$, and α . We assign gamma priors with shape parameter equal to 0.001 and rate parameter equal to 1,000 to the smoothing parameters κ and τ . We assume that $w_{st} \sim \text{Bernoulli}(0.5)$ for $s = 1, \dots, n$ and $t = 1, \dots, T$. We assign independent $\text{Bernoulli}(0.1)$ priors to the basis vector indicator variables $I_{\gamma j}$ and $I_{\delta j}$ for $j = 1, \dots, q$. This prior is appealing since it corresponds to the prior belief that the fixed effects are sufficient to account for data, and this prior can prevent our method from producing artifactual spatial structure in the posterior.

We fit our ZICOMP model by using our hybrid Monte Carlo algorithm illustrated in Section 4.3. We generate posterior sample paths of length at least 2 million in all cases to ensure that the Monte Carlo standard errors calculated by the batch means method (Jones et al., 2006; Flegal et al., 2008) are sufficiently small. We use normal proposals for $\boldsymbol{\beta}_1$, $\boldsymbol{\beta}_2$, $\boldsymbol{\zeta}$, and α and adapt proposal covariance matrices using the Log-Adaptive Proposal algorithm (Shaby and Wells, 2011). We use swapping proposals for w_{st} , $I_{\gamma j}$, and $I_{\delta j}$.

5.1 Data simulated from the full model

We create a data set by first setting $\kappa = \tau = 1$ and simulating random effects according to $\boldsymbol{\gamma} \sim \text{Normal}_{25}(\mathbf{0}, \mathbf{Q}_B^{-1})$ and $\boldsymbol{\delta} \sim \text{Normal}_{25}(\mathbf{0}, \mathbf{Q}_B^{-1})$. We generate response values under the following model:

$$\begin{aligned}\text{logit}(\pi_{st}) &= \mathbf{X}_{st}^\top \boldsymbol{\beta}_1 \\ \log(\eta_{st}) &= \mathbf{X}_{st}^\top \boldsymbol{\beta}_2 + \mathbf{B}_s^\top \boldsymbol{\gamma} + \mathbf{M}_t^\top \boldsymbol{\zeta} \\ \log(\nu_s) &= \alpha + \mathbf{B}_s^\top \boldsymbol{\delta}, \\ s &= 1, \dots, 900; t = 1, \dots, 24,\end{aligned}$$

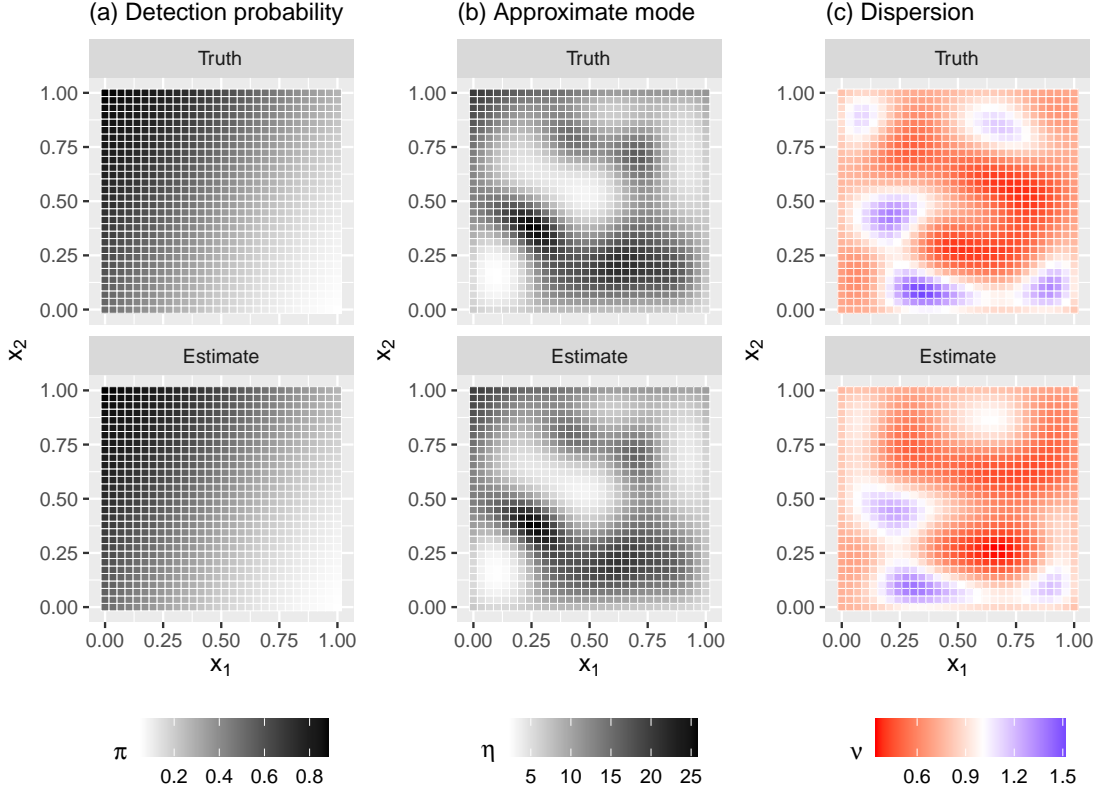


Figure 2: (a) True and estimated values of the detection probability π_{st} for $t = 1$. (b) True and estimated values of approximate mode η_{st} for $t = 1$. (c) True and estimated values of dispersion ν_s .

where $\beta_1 = (0, -3, 2)^\top$, $\beta_2 = (2, -0.5, 1)^\top$, $\zeta = (0, 0, 0, 0, 0, 0, 0.1, 0.2, 0.5, 0.4, 0.3)^\top$, and $\alpha = -0.3$. We fit our ZICOMP model with 50 eigenvectors to the simulated data set. We use more basis vectors than the truth to assess how our basis vector selection approach performs.

We see that the estimated posterior medians of the model parameters are close to the true values. All of their 95% highest posterior density (HPD) intervals cover the true values. To validate the performance more thoroughly, we apply our model to 100 simulated data sets and estimate coverage rates and type I and II error rates based on 95% HPD intervals. We observe 90.8–99.0% for the coverage rates of all parameters, 1.0–9.2% for type I error rates of parameters whose true values are zeros, and 0.0–2.0% for type II error rates of parameters whose true values are nonzero. This shows that our approach performs reliably.

For the spatial effects in $\boldsymbol{\eta}$, we observe that 22 basis vectors have estimated posterior probabilities of 0.5 and above. For the spatial effects in $\boldsymbol{\nu}$, we see that 13 basis vectors have estimated posterior probabilities of at least 0.5. The selected basis vectors are all true basis vectors. The unselected ones among the true basis vectors are found to have true basis coefficient values close to 0. This shows that our methodology performs reliably in selecting important basis vectors.

Figure 2 presents maps of true and estimated values for the detection probability π_{st} , approximate mode η_{st} , and dispersion ν_s for $t = 1$. Similar results are observed for $t = 2, \dots, 24$. We see that the estimated spatial patterns closely mirror the true spatial distributions. This shows that our approach recovers well the underlying spatial patterns in the data.

5.2 Data simulated from simpler models

We simulate a data set from each of the following models.

(ii) Model with constant dispersion:	$\text{logit}(\pi_{st}) = \mathbf{X}_{st}^\top \boldsymbol{\beta}_1$ $\log(\eta_{st}) = \mathbf{X}_{st}^\top \boldsymbol{\beta}_2 + \mathbf{B}_s^\top \boldsymbol{\gamma} + \mathbf{M}_t^\top \boldsymbol{\zeta}$ $\log(\nu_s) = \alpha$
(iii) Model with fixed effects only:	$\text{logit}(\pi_{st}) = \mathbf{X}_{st}^\top \boldsymbol{\beta}_1$ $\log(\eta_{st}) = \mathbf{X}_{st}^\top \boldsymbol{\beta}_2 + \mathbf{M}_t^\top \boldsymbol{\zeta}$ $\log(\nu_s) = \alpha$
(iv) Model with covariate effects only:	$\text{logit}(\pi_{st}) = \mathbf{X}_{st}^\top \boldsymbol{\beta}_1$ $\log(\eta_{st}) = \mathbf{X}_{st}^\top \boldsymbol{\beta}_2$ $\log(\nu_s) = \alpha$ $s = 1, \dots, 900; t = 1, \dots, 24,$

where $\boldsymbol{\gamma} \sim \text{Normal}_{25}(\mathbf{0}, \mathbf{Q}_B^{-1}/\kappa)$. We fit our ZICOMP model with 50 eigenvectors to these three simulated data sets. The aim of this simulation experiment is to see if our method-

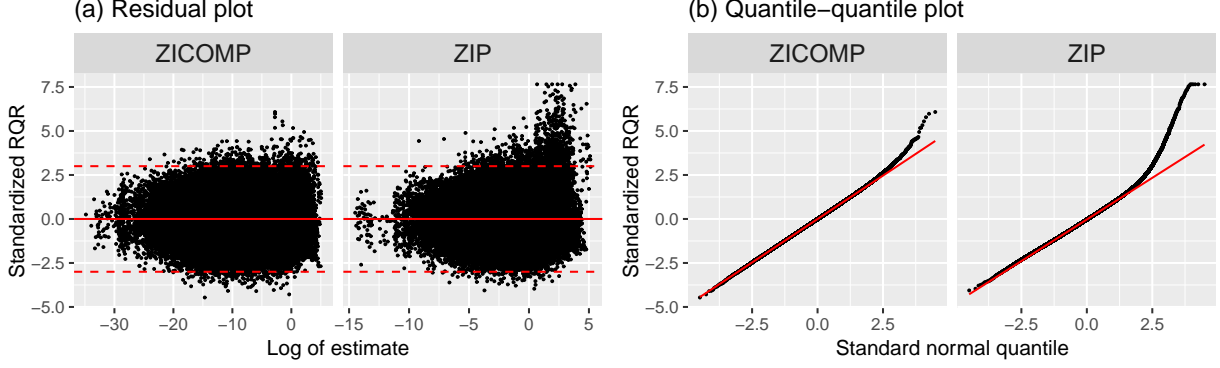


Figure 3: (a) Residual plots for the RQRs stemming from our ZICOMP model and the ZIP model. (b) Quantile-quantile plots for our ZICOMP model and the ZIP model. Our ZICOMP model fits the data much better than the ZIP model.

ology produces artifactual spatial or temporal structures in the posterior.

We observe that the estimated posterior medians of the model parameters are close to the simulated true values. All of their 95% HPD intervals cover the true values. When the true model is Model (ii), the fitted model correctly suggests that there is evident spatial dependence in $\boldsymbol{\eta}$ while there is no spatial variation in $\boldsymbol{\nu}$. For the spatial effects in $\boldsymbol{\eta}$, we observe that 23 basis vectors have estimated posterior probabilities of 0.5 and above. For the spatial effects in $\boldsymbol{\nu}$, none of the basis vectors have estimated posterior probabilities of 0.5 and above.

When the true models are Model (ii) and (iv), the fitted models correctly indicate that there is spatial variation in neither $\boldsymbol{\eta}$ nor $\boldsymbol{\nu}$. We observe that none of the basis vectors have estimated posterior probabilities of 0.5 and above. For the data simulated from Model (iv), all of the 95% HPD intervals for $\boldsymbol{\zeta}$ cover 0. This correctly suggests that there is no temporal effect evident in the data. In summary, our method effectively avoids overfitting and provides accurate inference for all parameters.

6 Application to vaccine refusal data

Now we apply our proposed methodology to the vaccine refusal data described in Section 2. We use 400 basis vectors so the fit can accommodate a rich spatial structure, if necessary. We use the same priors and proposal distributions as those given in Section 5.

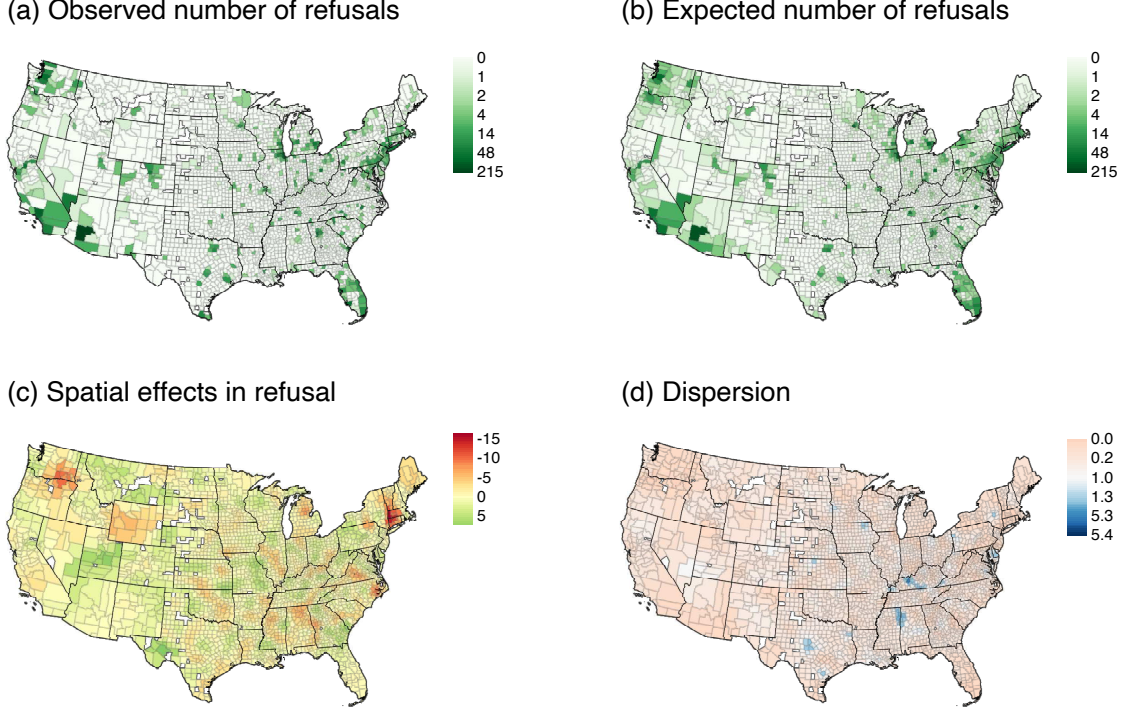


Figure 4: (a) The observed number of vaccine refusal cases in December 2015. (b) Estimates of the mean number of cases in December 2015. (c) Estimates of the spatial effects in refusal. Negative effects in red are associated with decrease in refusal while positive effects in green are associated with increase in refusal. (d) Estimates of dispersion. The red means over-dispersion while the blue mean under-dispersion. Note: The reason for our choice of scale is that the data are zero-inflated and only a few counties have large counts.

For comparison we also fit a zero-inflated Poisson (ZIP) regression model. The ZIP model describes the count process using the Poisson distribution with means equal to $\mu_{st} = \exp(\mathbf{X}_{st}^\top \boldsymbol{\beta}_2 + \mathbf{B}_s^\top \boldsymbol{\gamma} + \mathbf{M}_t^\top \boldsymbol{\zeta})$ and assumes equi-dispersion. We compare our ZICOMP model and the ZIP model via residual diagnosis. For these count data, the distribution of the standardized residuals is far from normal even though the model is well specified. And so we use randomized quantile residuals (RQRs), which have been shown to have low type I error rates and high statistical power for detecting model misspecification for count models, including zero-inflated models (Dunn and Smyth, 1996; Feng et al., 2020). Figure 3 shows residual plots for the RQRs stemming from our ZICOMP model fit and the ZIP model fit. The ZIP model produces infinite values of RQR that were excluded from the plots. We

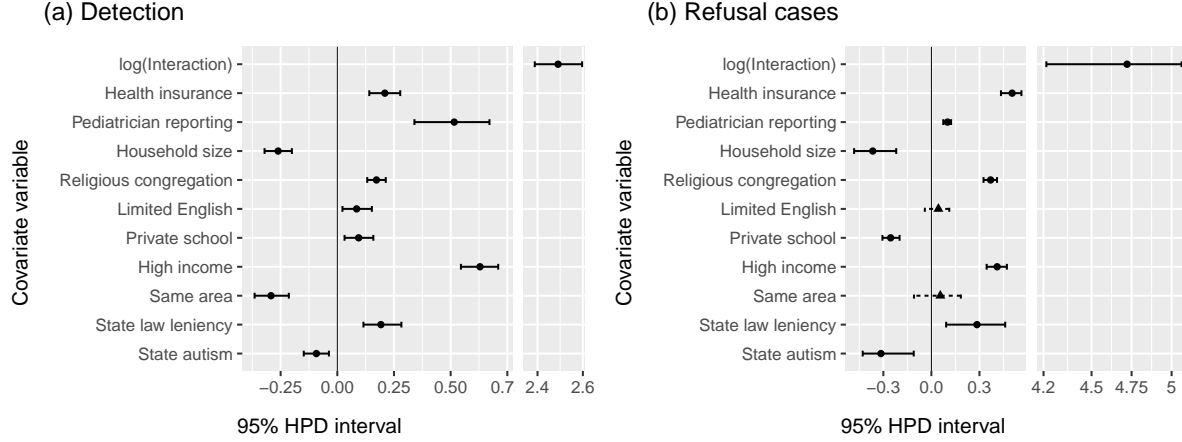


Figure 5: Estimated posterior medians (shaded dots or triangles) and 95% HPD intervals (horizontal solid or dashed bars) for covariate coefficients. The shaded dot and horizontal solid bar represent that the HPD interval does not include zero. The triangle and horizontal dashed bar represent that the HPD interval includes zero.

see that our ZICOMP model fits the data much better than the ZIP model. This suggests that we should allow for flexibility in modeling the dispersion of the vaccine refusal data.

Figure 4 (b) shows the estimated mean incidences of refusal under perfect detection in December 2015. To obtain the mean estimates, we simulate 10,000 response values from the fitted model and average them for each county. The spatial pattern of the mean is similar to the pattern for the observed counts presented in Figure 4 (a). We observe high incidences of refusal, on average, in the Northwest, Southwest, and Northeast regions of the United States, Florida, and the area around Lake Michigan.

Figure 4 (c) presents the estimates of the spatial effects in vaccine refusal. Positive effects (in green) are associated with increased refusal while negative effects (in red) are associated with decreased refusal. This spatial pattern may have been produced by some unobserved spatially-structured variables that are associated with refusal. Alternatively, it may have been produced by social influence, in which vaccination behavior is contagious and diffuses between neighboring areas, producing refusal clusters (Alvarez–Zuzek et al., 2022).

Figure 4 (c) displays the estimates of dispersion. We find evidence of spatial variation in the dispersion. Some areas have over-dispersed counts and some have under-dispersed

counts. For the month effects, we used January for a reference month. We find that people are less likely to refuse to vaccinate their children in March to August while people are more likely to refuse to vaccinate their children in September to December, compared to January.

Figure 5 (a) displays the estimated posterior medians and 95% HPD intervals for the regression coefficients for detection of vaccine refusal. We find that all healthcare-related measurement variables are predictive of refusal. Physician-patient interaction is overwhelmingly predictive. Among demographic or socioeconomic variables, we observe that communities with small household sizes, religions historically opposed to vaccination, limited proficiency in English, high rates of private school attendance, high incomes, lack of continuity of care, high leniency in the state’s vaccination laws, and low incidence of autism are likely to have reported refusals.

Figure 5 (b) presents the estimates and 95% HPD intervals for the regression coefficients for refusal cases. Given perfect detection, we see that communities with increased access to care, high insurance coverage, high likelihood of physician reporting, small household sizes, groups historically opposed to vaccination, low rates of private school attendance, high incomes, high leniency in state vaccination laws, and low incidence of autism are more likely to refuse to vaccinate their children.

7 Discussion

In this article we proposed a new, flexible ZICOMP regression model for examining the occurrence of childhood vaccine refusal in the United States. We also proposed several computational approaches that provide computational efficiency in carrying out Bayesian inference for our model. Our methodology has several attractive features. First, it addresses potential zero inflation relative to a standard count distribution. This allows us to account for imperfect detection of refusal cases and infer the refusal distribution under perfect detection. Our model also accounts for the underlying spatial pattern in vaccine refusal while correctly accommodating spatially-varying dispersion, which could not be done using previous models. Our approach could be useful in many disciplines, such as

ecology, agriculture, criminology, medicine, and public health studies where zero-inflated spatial data are commonly encountered (cf. Ratcliffe and Mccord, 2007; Neelon et al., 2016; Lyashevskaya et al., 2016).

The vaccine refusal analysis revealed several important findings. First, communities that have religions historically opposed to vaccination, have high incomes, and live in states with permissive vaccination laws are more likely to have high incidence of refusal. These associations have been reported in earlier studies (cf. Omer et al., 2006; Salmon et al., 2015; McKee and Bohannon, 2016). We also found that communities with large family sizes, high rates of private school attendance, and high incidence of autism are more likely to have low incidence of refusal. Our analysis indicated that vaccine refusal exhibits spatial dependence that is not explained by the set of our covariates. This spatial dependence may have been produced by some unobserved spatially-structured variables. This hypothesis means that the clustering in vaccine refusal only reflects spatial clustering in underlying drivers. Alternatively, the spatial dependence may have been caused by diffusion of vaccination behavior between neighboring areas. Identifying the source of clustering is important for effectively alleviating the clustering and reducing the risk of disease outbreaks (Alvarez–Zuzek et al., 2022). Our findings suggest that refusal behavior may be contagious.

We conclude with a few crucial caveats. We used observational data and therefore can infer only associations between vaccine refusal behavior and the covariates. Readers interested in developing interventions for improving public health would expect to be informed about causal effects. When we interpret our results, consideration must be taken to prevent the ecological inference fallacy. We carry out statistical inference at the county-level and try to infer ecological factors on vaccine refusal rather than individual factors. Our Markov chains mix slowly, which inspired us to use reparameterization techniques. However, we still need to generate long sample paths to ensure convergence of the chains. Further improvement in computing may be an interesting topic for future research.

References

- Alvarez–Zuzek, L. G., Zipfel, C., and Bansal, S. (2022). Spatial clustering in vaccination hesitancy: the role of social influence and social selection. *PLoS Computational Biology*.
- Benson, A. and Friel, N. (2021). Bayesian inference, model selection and likelihood estimation using fast rejection sampling: the Conway-Maxwell-Poisson distribution. *Bayesian Analysis*, 16:905–931.
- Besag, J. (1974). Spatial interaction and the statistical analysis of lattice systems. *Journal of the Royal Statistical Society: Series B*, 36:192–225.
- Chanialidis, C., Evers, L., Neocleous, T., and Nobile, A. (2018). Efficient Bayesian inference for COM-Poisson regression models. *Statistics and Computing*, 28:595–608.
- Conway, R. W. and Maxwell, W. L. (1962). Network dispatching by the shortest-operation discipline. *Operations Research*, 10:51–73.
- Dunn, P. K. and Smyth, G. K. (1996). Randomized quantile residuals. *Journal of Computational and Graphical Statistics*, 5:236–244.
- Feng, C., Feng, C., Li, L., and Sadeghpour, A. (2020). A comparison of residual diagnosis tools for diagnosing regression models for count data. *BMC Medical Research Methodology*, 20:1–21.
- Flegal, J. M., Haran, M., and Jones, G. L. (2008). Markov chain Monte Carlo: Can we trust the third significant figure? *Statistical Science*, 23:250–260.
- Frieden, T. R., Jaffe, D. W. H., Kent, C. K., Leahy, M. A., Martinroe, J. C., Spriggs, S. R., Starr, T. M., Doan, Q. M., King, P. H., Roper, W. L., Hill, C., Boulton, C. L. M., Arbor, A., Caine, M. A. V., Fielding, I. E. J., Jones, T. F., Khabbaz, T. F. R., Maki, G. G. D., Quinlisk, W. P., Moines, D., Remington, I. L. P., and Schaffner, W. W. (2014). National, state, and selected local area vaccination coverage among children aged 19–35 months — United States, 2013. *Morbidity and Mortality Weekly Report*, 63:748.

- Glanz, J. M., Newcomer, S. R., Narwaney, K. J., Hambidge, S. J., Daley, M. F., Wagner, N. M., McClure, D. L., Xu, S., Rowhani-Rahbar, A., Lee, G. M., Nelson, J. C., Donahue, J. G., Naleway, A. L., Nordin, J. D., Lugg, M. M., and Weintraub, E. S. (2013). A population-based cohort study of undervaccination in 8 managed care organizations across the United States. *JAMA Pediatrics*, 167:274–281.
- Godsill, S. J. (2012). On the relationship between Markov chain Monte Carlo methods for model uncertainty. *Journal of Computational and Graphical Statistics*, 10:230–248.
- Green, P. J. (1995). Reversible jump Markov chain Monte Carlo computation and Bayesian model determination. *Biometrika*, 82:711–732.
- Guikema, S. D. and Goffelt, J. P. (2008). A flexible count data regression model for risk analysis. *Risk Analysis*, 28:213–223.
- Hanks, E. M., Schliep, E. M., Hooten, M. B., and Hoeting, J. A. (2015). Restricted spatial regression in practice: Geostatistical models, confounding, and robustness under model misspecification. *Environmetrics*, 26:243–254.
- Haran, M. (2011). Gaussian random field models for spatial data. *Handbook of Markov Chain Monte Carlo*, pages 449–478.
- Hill, H. A., Elam-Evans, L. D., Yankey, D., Singleton, J. A., and Kolasa, M. (2015). National, state, and selected local area vaccination coverage among children aged 19–35 months — united states, 2014. *Morbidity and Mortality Weekly Report*, 64:889–896.
- Hughes, J. (2017). Spatial regression and the Bayesian filter. *arXiv preprint arXiv:1706.04651*.
- Hughes, J. and Haran, M. (2013). Dimension reduction and alleviation of confounding for spatial generalized linear mixed models. *Journal of the Royal Statistical Society: Series B (Statistical Methodology)*, 75:139–159.

- Jones, G. L., Haran, M., Caffo, B. S., and Neath, R. (2006). Fixed-width output analysis for Markov chain Monte Carlo. *Journal of the American Statistical Association*, 101:1537–1547.
- Kang, B., Goldlust, S., Lee, E. C., Hughes, J., Bansal, S., and Haran, M. (2022). Spatial distribution and determinants of childhood vaccination refusal in the United States. *arXiv preprint arXiv:2211.03763*.
- Khan, K. and Calder, C. A. (2020). Restricted spatial regression methods: implications for inference. *Journal of the American Statistical Association*, 0:1–13.
- Lambert, D. (1992). Zero-inflated Poisson regression, with an application to defects in manufacturing. *Technometrics*, 34:1–14.
- Lieu, T. A., Ray, G. T., Klein, N. P., Chung, C., and Kulldorff, M. (2015). Geographic clusters in underimmunization and vaccine refusal. *Pediatrics*, 135:280–289.
- Lyashevskaya, O., Brus, D. J., and van der Meer, J. (2016). Mapping species abundance by a spatial zero-inflated Poisson model: a case study in the Wadden Sea, the Netherlands. *Ecology and Evolution*, 6:532–543.
- McCarthy, N. L., Irving, S., Donahue, J. G., Weintraub, E., Gee, J., Belongia, E., and Baggs, J. (2013). Vaccination coverage levels among children enrolled in the Vaccine Safety Datalink. *Vaccine*, 31:5822–5826.
- McKee, C. and Bohannon, K. (2016). Exploring the reasons behind parental refusal of vaccines. *The Journal of Pediatric Pharmacology and Therapeutics*, 21:104–109.
- Murray, I., Ghahramani, Z., and Mackay, D. J. C. (2006). MCMC for doubly-intractable distributions. pages 359–366.
- Neelon, B., O’Malley, A. J., and Smith, V. A. (2016). Modeling zero-modified count and semicontinuous data in health services research Part 1: background and overview. *Statistics in Medicine*, 35:5070–5093.

- Omer, S. B., Pan, W. K., Halsey, N. A., Stokley, S., Moulton, L. H., Navar, A. M., Pierce, M., and Salmon, D. A. (2006). Nonmedical exemptions to school immunization requirements: secular trends and association of state policies with pertussis incidence. *JAMA*, 296:1757–1763.
- Patel, M., Lee, A. D., Clemmons, N. S., Redd, S. B., Poser, S., Blog, D., Zucker, J. R., Leung, J., Link-Gelles, R., Pham, H., Arciuolo, R. J., Rausch-Phung, E., Bankamp, B., Rota, P. A., Weinbaum, C. M., and Gastañaduy, P. A. (2019). National update on measles cases and outbreaks — United States, January 1 – October 1, 2019. *Morbidity and Mortality Weekly Report*, 68:893–896.
- Phadke, V. K., Bednarczyk, R. A., Salmon, D. A., and Omer, S. B. (2016). Association between vaccine refusal and vaccine-preventable diseases in the United States: A review of measles and pertussis. *JAMA*, 315:1149–1158.
- Ratcliffe, J. H. and Mccord, E. S. (2007). A micro-spatial analysis of the demographic and criminogenic environment of drug markets in philadelphia. *Australian and New Zealand Journal of Criminology*, 40:43–63.
- Reich, B. J., Hodges, J. S., and Zadnik, V. (2006). Effects of residual smoothing on the posterior of the fixed effects in disease-mapping models. *Biometrics*, 62:1197–1206.
- Salmon, D. A., Dudley, M. Z., Glanz, J. M., and Omer, S. B. (2015). Vaccine hesitancy: Causes, consequences, and a call to action. *Vaccine*, 33:D66–D71.
- Salmon, D. A., Smith, P. J., Navar, A. M., Pan, W. K., Omer, S. B., Singleton, J. A., and Halsey, N. A. (2006). Measuring Immunization Coverage among Preschool Children: Past, Present, and Future Opportunities. *Epidemiologic Reviews*, 28:27–40.
- Shaby, B. and Wells, M. T. (2011). Exploring an adaptive Metropolis algorithm. Technical report, Department of Statistical Science, Duke University.
- Shmueli, G., Minka, T. P., Kadane, J. B., Borle, S., and Boatwright, P. (2005). A useful distribution for fitting discrete data: Revival of the Conway–Maxwell–Poisson distribution. *Journal of the Royal Statistical Society: Series C*, 54:127–142.

- Smith, P. J., Chu, S. Y., and Barker, L. E. (2004). Children who have received no vaccines: who are they and where do they live? *Pediatrics*, 114:187–195.
- Zimmerman, D. L. and Hoef, J. M. V. (2021). On deconfounding spatial confounding in linear models. *The American Statistician*, 00:1–9.
- Zipfel, C. M., Garnier, R., Kuney, M. C., and Bansal, S. (2020). The landscape of childhood vaccine exemptions in the United States. *Scientific Data*, 7:1–7.